

---

# Synthesis and Characterization of Silicon Nanoparticles from Coal Fly Ash Using Ultrasonication as a Battery Anode

Robiansyah<sup>1,2</sup>, Yohandri Bow<sup>3,\*</sup> & Tresna Dewi<sup>4</sup>

<sup>1</sup>Department of Renewable Energy Engineering, Politeknik Negeri Sriwijaya, Jl. Sriwijaya Negara Bukit Besar, Palembang, 30139, Indonesia

<sup>2</sup>Department of Technical Plant, Unit of Quality Assurance, PT. Semen Baturaja, Tbk., Ogan Komering Ulu, 32115, Indonesia

<sup>3</sup>Department of Energy Engineering, Politeknik Negeri Sriwijaya, Jl. Sriwijaya Negara Bukit Besar, Palembang, 30139, Indonesia

<sup>4</sup>Department of Electrical Engineering, Politeknik Negeri Sriwijaya, Jl. Sriwijaya Negara Bukit Besar, Palembang, 30139, Indonesia

## Email address:

yohandri@polsri.ac.id

\*Corresponding author

## To cite this article:

Robiansyah, Bow, Y., & Dewi, T. (2024). Synthesis and Characterization of Silicon Nanoparticles from Coal Fly Ash Using Ultrasonication as a Battery Anode. *International Journal of Research in Vocational Studies (IJRVOCAS)*, 4(2), 23–32. <https://doi.org/10.53893/ijrvocas.v4i2.282>

**Received:** 05 21, 2024; **Accepted:** 07 02, 2024; **Published:** 08 31, 2024

---

**Abstract:** Fly ash, a byproduct of coal combustion, is rich in silica, alumina, and other minerals, making it a valuable resource for extracting high-purity silicon. The synthesis of silicon nanoparticles from coal fly ash involves several critical steps, including the extraction of silica (SiO<sub>2</sub>) via the sol-gel method, reduction of silica to silicon using the metallothermic method, and subsequent ultrasonication to achieve nanoscale particles. Studies have shown that fly ash can contain up to 49.21% silica, which can be further purified to 93.52% via chemical extraction methods such as acid leaching and alkali dissolution. The reduction of silica to silicon is carried out using the metallothermic method, which involves the use of magnesium-reducing agents to convert SiO<sub>2</sub> to elemental silicon. This process produces silicon with a purity of about 61.3%, which can be further increased through ultrasonication. Ultrasonication is a technique that uses high-frequency sound waves to break particles into smaller sizes, resulting in more uniform and homogeneous nanoparticles. In this study, ultrasonication for 60 and 120 min reduced the average particle size of silicon from 208.94 nm to 58.87 nm and 20.13 nm, respectively, and increased the silicon content to 74.6% and 72.7%. X-ray diffraction (XRD) and distribution particle analyses confirmed the particle size reduction and homogeneity of silicon nanoparticles, indicating the effectiveness of ultrasonication in producing high-quality silicon nanoparticles. The synthesized silicon nanoparticles have significant potential applications, particularly as anode materials in lithium-ion batteries, due to their increased surface area and improved electrochemical properties. Furthermore, the use of fly ash as a raw material for the synthesis of silicon nanoparticles not only provides a cost-effective and environmentally friendly alternative to traditional silica sources but also helps in reducing the environmental impact of fly ash disposal. The integration of the methods and findings of this study underscores the feasibility and benefits of using coal fly ash for the sustainable production of silicon nanoparticles, which can be utilized in energy storage as anode materials in lithium-ion batteries.

**Keywords:** characterization, silicon nanoparticle, fly ash, ultrasonication, battery anode

---

## 1. Introduction

Coal utilization in steam power plants produces various by-products, including fly ash, bottom ash, boiler slag, flue gas desulfurization residue, and fluidized bed combustion ash, with fly ash being the dominant constituent [1]. The

main constituent of coal combustion ash is fly ash, which consists of spherical particles with diameters varying from 0.1 μm to > 100 μm [2]. The composition of fly ash is contingent upon the combustion conditions [3]. This ash

content may vary depending on the source of coal and the combustion process used by power plants.

The environmental impact needs to be considered, as power plants that use a significant amount of coal need to be considered. Coal used as fuel can produce ash as a combustion residue. Ash can be generated as hazardous waste in the forms of bottom ash and fly ash [4]. Utilizing fly ash can help us lessen the garbage that industry power plants produce, which will diminish its detrimental effects on the environment.

Thanks to advancements in research and development technology, fly ash is currently used in metallurgy, adsorbents, fertilizers, geopolymers, ceramics and buildings, and adsorbents [5-6]. In the construction industry, fly ash is added to cement or concrete mixtures as a substitute for cement, which provides benefits such as economic effectiveness, environmental sustainability, and structural strength [7].

Fly ash is composed of many porous oxides, including  $\text{SiO}_2$ ,  $\text{Al}_2\text{O}_3$ ,  $\text{Fe}_2\text{O}_3$ ,  $\text{MgO}$ , and  $\text{CaO}$ , and has a hollow structure [8]. The main content of fly ash is silicon dioxide ( $\text{SiO}_2$ ), an alternative material to produce silicon (Si). Silicon has industrial and potential applications in high-tech fields, such as semiconductors, nanoelectronics, biotechnology, and energy storage [9].

One of the main applications of silicon is recent technological advances in energy storage [10] and semiconductors in solar panels, which can produce electricity when photons from sunlight hit the panels [11]. Silicon can also be used as a substitute for graphite as the anode material in lithium-ion batteries for energy storage. Due to its high theoretical capacity features (4200 mAh/g Si vs 372 mAh/g graphite) and shallow potential values, silicon is considered a far better anode than graphite [12-13].

Battery life depends on the technology and quality of the material used [14]. Silicon as an anode material can be expanded by improving its characteristics. One way to fix these characteristics is to synthesize nano-sized silicon. Synthesis of silicon nanoparticles, which have dimensions ranging from 1 to 100 nm, can further improve the performance of silicon as an anode material. Nanoparticles have all exterior dimensions in the nanoscale and can be spherical, cylindrical, conical, tubular, hollow core, spiral, or have irregular morphology, among other shapes, sizes, and architectures [15-16].

There are two types of methodologies for synthesizing nanoparticles: top-down and bottom-up. Techniques like thermal decomposition, laser ablation, and ultrasonication have been introduced for top-down approaches to break down bulk materials to the nanoscale [17]. In the synthesis process, ultrasonication is a valuable technique for adjusting the size and dispersion of nanomaterials [18].

In this study, silicon nanoparticles were synthesized using the sol-gel method to extract silica from coal fly ash, followed by metallothermic reduction and ultrasonication to achieve nanoscale silicon. The silicon obtained from this

synthesis process can be used as anode material in batteries, especially lithium-ion batteries, which are currently being developed, to increase the energy storage capacity needed in renewable energy.

X-ray diffraction (XRD) and Scanning Electron Microscopy (SEM) were used to investigate the characteristics of the silicon nanoparticles produced from this extraction and the effect of ultrasonication time on particle morphology and size. This innovative approach not only provides a sustainable solution to manage coal combustion by-products but also contributes to the advancement of energy storage technology, thereby promoting environmental sustainability and technological advancement.

## 2. Material and Method

### 2.1. Material

The materials used were fly ash and demineralized water obtained from PT Semen Baturaja Tbk. The fly ash used is a waste processed from one of these power plants in the fertilizer industry. Sodium hydroxide (NaOH 98%), hydrochloric acid (HCl 37%), magnesium powder (Mg 98%), and PEG 6000 were used as commercial chemicals from Merck.

### 2.2. Synthesis of Silicon Nanoparticles

The synthesis of silicon nanoparticles begins with fly ash silica extraction, silicon isolation and purification, and ultrasonication using an ultrasonic batch.

#### 2.2.1. Silica Extraction

Samples of fly ash were immersed in hot water for two hours. A solution of 500 mL of 1 M HCl and 100 grams of fly ash was heated to 90 °C for four hours while continuously stirring. After filtering the mixture, the residue was cleaned with hot, distilled water until it became neutral, and it was then baked for 12 hours at 110 °C. A magnetic stirrer added 150 mL of 3 M NaOH, and the mixture was agitated for four hours at 90 °C at 150 rpm. The solution was balanced after using Whatman 41 paper to filter the mixture, collecting the filtrate, and adding 1 M HCl to reach pH 7. After letting the solution remain for eighteen hours, the residue was extracted, cleaned in hot distilled water, and dried for twelve hours at 110 °C in an oven. Ten grams of silica were placed in an Erlenmeyer, and 20 milliliters of 37% HCl were added to a hotplate set at 90 °C for three hours, with occasional stirring. The solution was allowed to stand until the temperature dropped, filtered and washed with distilled water until the pH was neutral, and then dried at 110 °C for 3 hours.

#### 2.2.2. Silicon Isolation

The extracted silica was added to magnesium powder in a ratio of 1:0.8, homogenized, and dried using a furnace for 3 hours at 650 °C. After adding the reduced sample, 150 mL of 2 M HCl was heated to 80 °C for three hours while stirred with a

magnetic stirrer. The mixture was then cooled, filtered through Whatman 41 to produce silicon solids, and dried after being rinsed with distilled water until it reached a neutral pH.

### 2.2.3. Ultrasonication

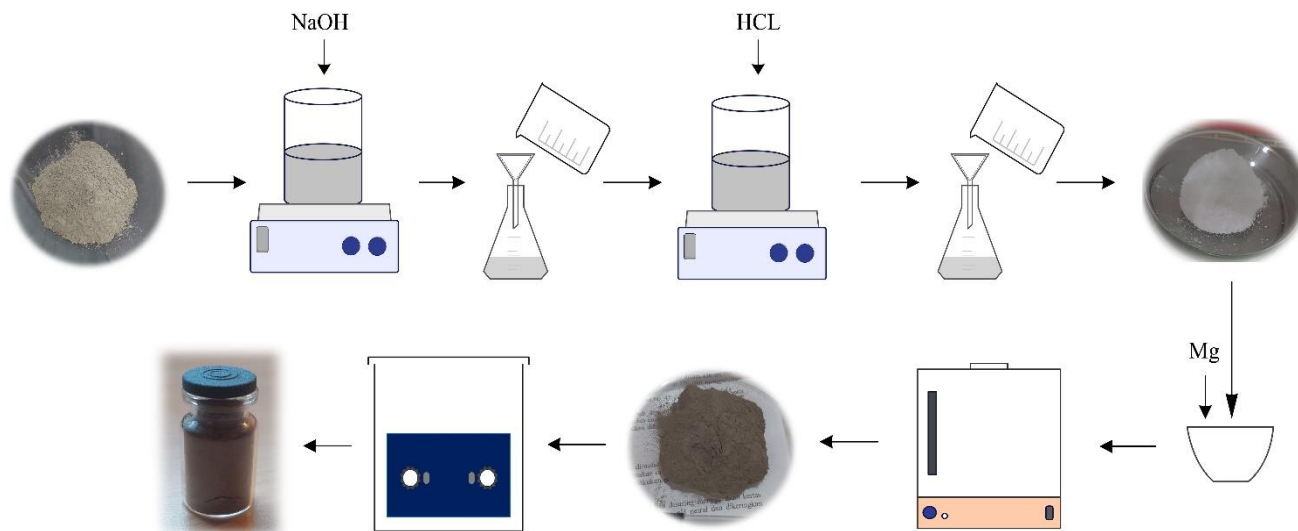


**Figure 1.** Flow diagram synthesis silicon nanoparticle from coal fly ash

PEG 6000 was heated to 105 °C for two hours. A 1:5 ratio dissolved the purified silicon in liquid PEG 6000. The mixture was agitated with a magnetic stirrer for fifteen minutes. The ultrasonication process was carried out using an ultrasonic bath with time variations of 60 and 120 minutes. The sonication results were dried using a furnace at 750 °C for three hours.

### 2.3. Characterization

The chemical makeup of fly ash and extracted silica was examined using X-ray fluorescence (XRF) ARL 9900 at 30 kV and 40 mA. X-ray diffraction (XRD) Pan Analytical Xpert 3 Powder XRD was used to examine the crystal size and structure of the silicon nanoparticles. The wavelength number was fixed at 0.1540 nm, and an angle between 20° and 90° was used for the analysis. Software Match3 is used for phase analysis using powder diffraction data.

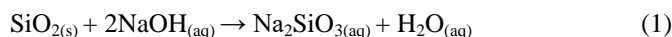
## 3. Result and Discussion

### 3.1. Synthesis of Silicon Nanoparticles

The synthesis of silicon nanoparticles begins with silica extraction, isolation, and purification of silicon, followed by ultrasonication with an ultrasonic bath to obtain silicon at a nanoscale size, as shown in Figure 1. Table 1 shows the silica content (SiO<sub>2</sub>) in fly ash samples after initial washing, with a silica content (SiO<sub>2</sub>) of 49.21%.

Silica from fly ash was extracted with 3 M NaOH solvent and precipitation using 1M HCl. NaOH solvent because it has strong alkaline properties compared to other types of

bases [19]. The reaction that occurs between silica (SiO<sub>2</sub>) in fly ash and NaOH is as follows:



From equation (1), the SiO<sub>2</sub> compounds in the fly ash will react with NaOH and produce a sodium silicate solution (Na<sub>2</sub>SiO<sub>3</sub>). SiO<sub>2</sub> is slightly acidic, so it can react with the base to produce salt and water. Zhang et al. (2018) state that the extraction process occurs due to the NaOH solvent dissolving silica (SiO<sub>2</sub>) within the fly ash capillaries. Fly ash is separated from a silica solution [20]. Furthermore, when reacting Na<sub>2</sub>SiO<sub>3</sub> with HCl, Na<sup>+</sup> ions and H<sup>+</sup> ions are exchanged with the reaction in equations 2 and 3.



At equations (2) and (3), the solution of NaSiO<sub>2</sub> will react with HCl. The reaction that occurs is a reaction between salt and acid, which is an intermediate reaction that produces H<sub>2</sub>SiO<sub>3</sub> and NaCl. At the end of the response, H<sub>2</sub>SiO<sub>3</sub> will turn into SiO<sub>2</sub> and water. The silica yield from this process stage is 93.52%, as shown in Table 1. The results were obtained by testing the sample using X-ray fluorescence (XRF). This is due to the diffusion process of Na<sup>+</sup> ions and other anions, which increases the silica content.

Silicon was isolated from extracted silica using the metallothermic method with magnesium (Mg) as a reductant. Magnesium is suitable for reducing silica to silicon due to its lower temperature, faster process, and high silicon yield [21]. Magnesiothermic reduction of silica (SiO<sub>2</sub>) will result in lower silicon (Si) material porousness compared to conventional reduction methods.

**Table 1.** Composition of fly ash and extraction silica

Compon ent	Fly ash (%)	Extracted silica (%)
SiO <sub>2</sub>	49.21	93.52
Al <sub>2</sub> O <sub>3</sub>	16.22	1.14
Fe <sub>2</sub> O <sub>3</sub>	5.49	1.17
K <sub>2</sub> O	0.50	0.06
CaO	7.37	0.93
MgO	1.72	1.08

Magnesium and oxygen in silica will react to produce magnesium oxide (MgO) as in the following equation:



semi-quantitative values by comparing the  $I/I_c$  values of the diffractogram standard sources from COD (Crystallography Open Database). The intensity obtained from the XRD test results at each angle of the 2-theta will be drawn as a diffractogram by comparing it to a standard diffractogram, and then the contents can be identified.

Figure 2 displays the silicon product's phase composition: 52.2% silicon and 47.8% for non-ultrasonic (TS) samples, 68.7% silicone and 31.3% for 60-minute ultrasonic samples (S60), and 66.3% silicone and 33.7% for 120-minute ultrasonic samples (S120) which is obtained from the interpretation of the XRD test results.

The chemical composition of the silicon product is displayed in Figure 2, together with additional components, such as Mg,

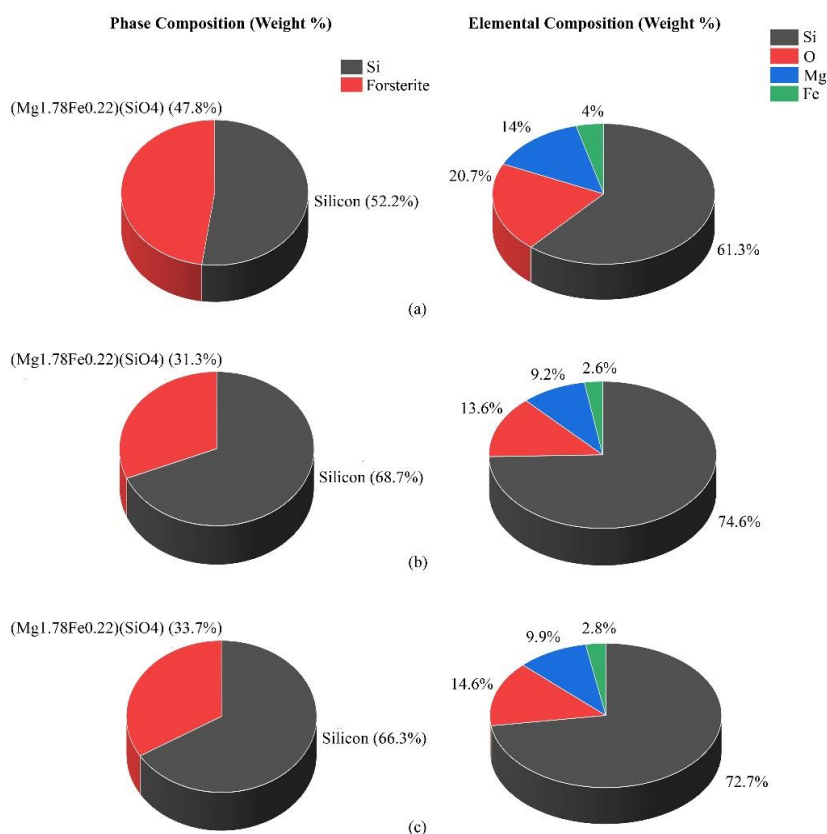


**Figure 2.** Phase and elemental composition of ultrasonication time variation: (a) 0 minutes, (b) 60 minutes, and (c) 120 minutes

The silica: magnesium ratio used is 1:0.8 in weight percent, a stoichiometric ratio. According to equation 4, two magnesium molecules are required to obtain one silicon molecule derived from 1 molecule of silica. The silicon product produced from this stage is ultrasonicated using a batch ultrasonic at a frequency of 37 kHz with time variations of 60 minutes and 120 minutes. Ultrasonication reduces the silicon's size produced from silicon extraction and isolation by utilizing the energy of ultrasonic waves.

Product quantification can be analyzed using XRD with the help of Match 3 software. This software presents

Si, O, and Fe, based on the results found in the Match 3 software. Mg, Si, and O are elements derived from the silicon separation reaction process, which theoretically forms an enstatite compound ( $\text{MgSiO}_3$ ) as an intermediate phase due to the reaction between MgO on the  $\text{SiO}_2$  surface, which then forms forsterite ( $\text{Mg}_2\text{SiO}_4$ ). The reaction is as follows:



(intermediate phase)

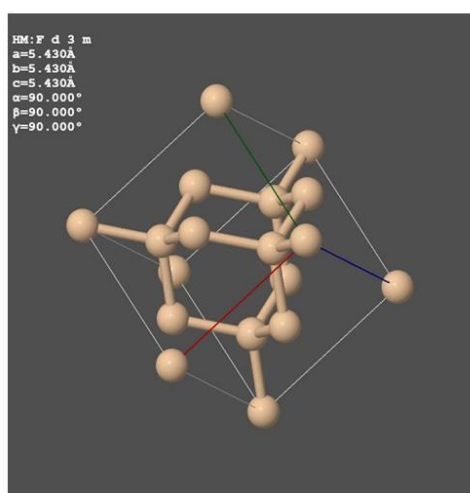


(forsterite)

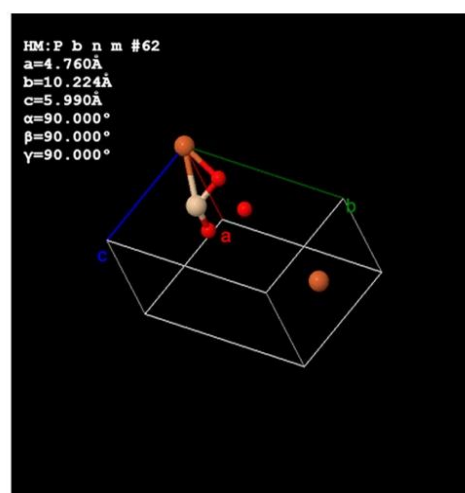
Based on Match 3 software, there is also an element of Fe with chemical compounds identified as  $Mg_{1.78}Fe_{0.22}SiO_4$ . This Fe element comes from the extracted silica content, which reacted with Mg during the silicon isolation process.

### 3.2. Characterization of Silicon Nanoparticles

XRD intensity data derived from samples can be used to determine the composition of the constituent elements by comparing the diffraction pattern measured with the known diffraction patterns of various crystalline structures of elements or compounds in the sample. By using Match3 software, in addition to knowing the elements contained therein, the composition of its contents can also be known in weight percent.



(a)



(b)

**Figure 3.** Crystal structure of the silicon phase (a) and forsterite phase (b)

Figure 2 shows the elemental content of each sample of sonication time variation. Four constituent elements exist: Si, Mg, O, and Fe. The effect of sonication can be seen from the increase in Si content for the sample with the need for sonication, which increases from 61.3% to 74.6%. With the increase in sonication time, the Si content decreases slightly from 74.6% to 72.7%.

The increase in Si content from the sonication time treatment is due to the calcination treatment of the sample at 750 °C for 3 hours at the final stage of the ultrasound process, which was not done by the sample without sonication. With this calcination, the metallothermic reaction between silica and magnesium occurs again, as in the silicon isolation process.

From the XRD test results, it is known that the synthesis carried out still has an impurity, where the synthesized silicone still has other elements or compounds, which affects the purity of the resulting product and will affect the use of

this silicone material in the future. This impurity is from the silica extraction and silicon purification processes that run poorly, with silicone purity as low as 74.6%.

XRD testing can also aim to determine the phase structure, degree of crystallinity, and crystallite size. Based on known analysis results, silicon samples have two material phases: silicon and forsterite. In Figure 3(a), which shows the cubic structure of the silicone phase, silicon atoms are regularly arranged in a cubic mesh. Silicon cube structures have characteristic features of the cube mesh, such as high symmetry and high atomic density, that affect the material properties associated with silicone use. Figure 3(a) shows that the crystallographic unit cells of silicone crystal structures showed the crystal mesh represented as two face-centered cubic lattices, with cubic sides a, b, and c, respectively 5,430 Å. The silicone crystallizes in the same

pattern as the diamond, in a structure that Ashcroft and Mermin called “two interpenetrating face-centered” cubic primitive lattices [22].

Figure 3(b) is an orthorhombic structure of the mineral forsterite phase, a crystal structure with an angled gap forming a triangle with three equally large angles. This material depends on its chemical composition and physical conditions, which have unique and valuable properties in electronics, crystallography, and engineering materials. In general, forsterite is found in the form of olivine minerals with  $Mg_2SiO_4$  compounds; the olivine-type silicate  $Mg_2SiO_4$  has an orthorhombic crystal structure with the space group Pbnm, in which four formula units are contained in the unit cell [23]. The crystallographic unit cells of forsterite crystal structures are  $a = 4.760 \text{ \AA}$ ,  $b = 10.224 \text{ \AA}$ , dan  $c = 5.990 \text{ \AA}$ .

The diffractogram analysis process uses Match 3 software,

which matches the data obtained from XRD diffraction with X-ray diffraction standards on the material. The X-ray diffraction standard comes from COD (Crystallography Open Database). The diffractograms of each silicon product produced can be seen in Figure 4. Based on Figure. 4, data were obtained on the silicon diffractogram pattern with sonication time variations of 0 minutes, 60 minutes, and 120 minutes. The silicon phase (red color) and the forsterite phase (green color), with the chemical compounds  $Mg_{1.78}Fe_{0.22}SiO_4$ .

An XRD test was used to identify the phase formed from each sample by comparing the 2-theta angle values in the  $10^\circ - 90^\circ$  angle measurement range. In Figure 3(a), the diffraction pattern formed at each 2-theta angle with its tip is matched with the database in the Match 3 software that contains the refraction pattern to identify the existing phase. The scan results show that the phase results are the silicone phase with a cubic structure and the forsterite phase with an orthorhombic structure with a structural appearance like in Figure 3. The same is true of the diffractogram on ultrasound time 60 minutes and 120 minutes, formed by each of the phase's silicone and forsterite phases consisting of the compound  $Mg_{1.78}Fe_{0.22}SiO_4$ .

In this study, ultrasound time does not influence material phase changes.

Measuring the described silicon's degree of crystallinity using the XRD data can yield the desired result. The degree of crystallinity measures a material's crystal content relative to its total amorphous and crystal surface area. The formula for calculating crystallinity degree is FWHM (Full Width at Half Maximum). The crystalline or amorphous fraction is calculated by multiplying FWHM by the intensity obtained from XRD. Using Origin software, the crystal curve area and the amorphous and crystalline areas can be calculated based on the XRD intensity data and the FWHM value. Table 2 shows the crystallinity values of the silicon synthesis samples with sonication time variation.

Table 2 shows that the degree of crystallinity decreases with sonication time. This is because silicon receives higher energy intensity during longer sonication, which can fracture the crystalline structure. The XRD diffractogram also confirms the decrease in the degree of crystallinity, as shown in Figure 4. It can be seen that with the sonication treatment of 60 minutes and 120 minutes, there is a decrease in the intensity of the 2-theta peaks at an angle of 28 degrees. With this decrease in intensity, the crystal area fraction also

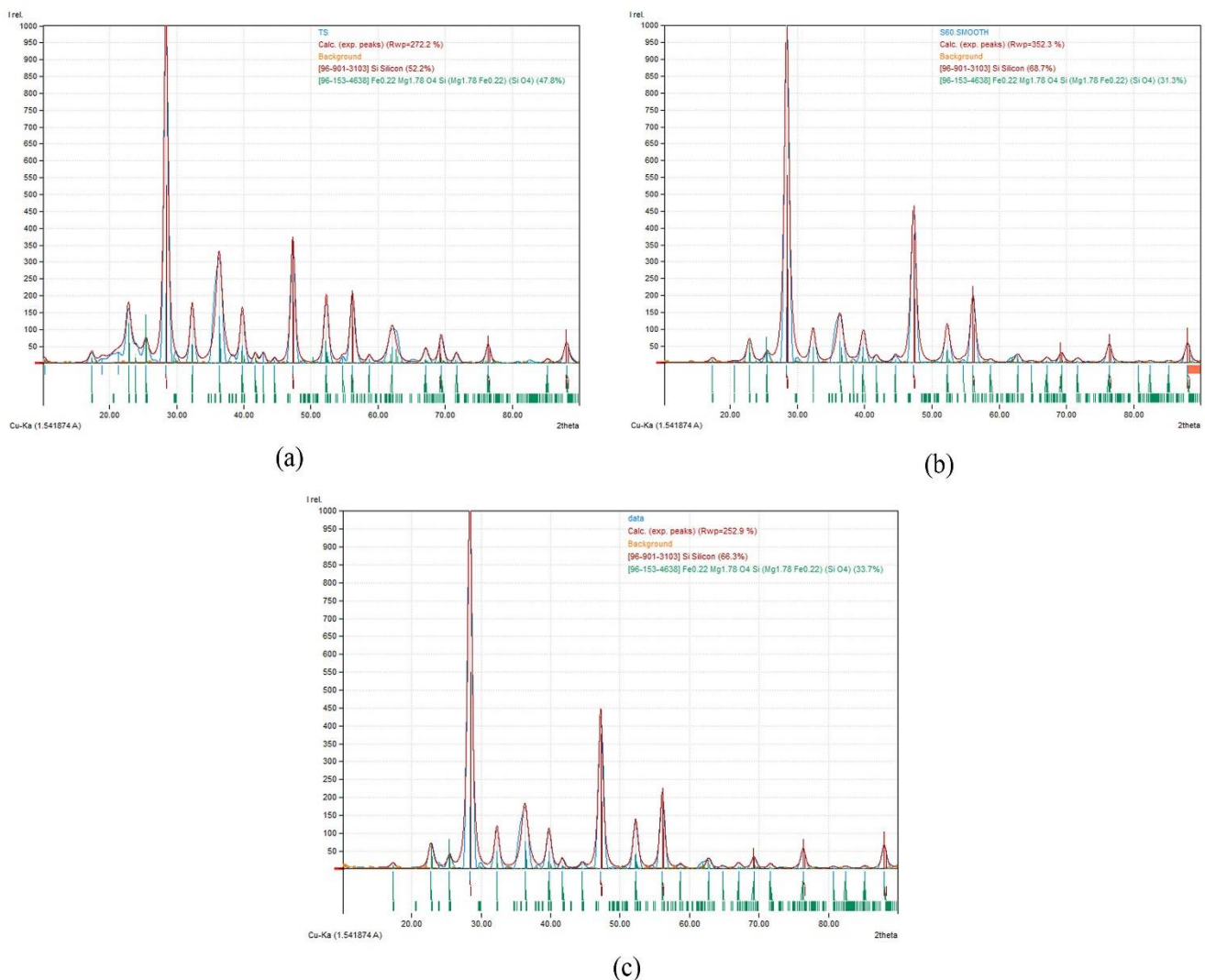


Figure 4. XRD pattern diffractograms of ultrasonication time variation: (a) 0 minutes, (b) 60 minutes, and (c) 120 minutes

becomes smaller, so the degree of crystallinity will eventually decrease.

Crystallinity in materials refers to the degree of structural order within a solid, impacting its properties. Various studies highlight the significance of crystallinity in different materials. For instance, the crystallinity of silicon embedded in silicon suboxides significantly influences the electrochemical performance of anode materials for lithium-ion batteries [24].

**Table 2.** Degree of crystallinity

Sample	Crystal Area	Crystal Area + Amorphous	Degree of Crystallinity
TS	36390.9	41653.1	87.4 %
S60	24561.6	28422.3	86.4 %
S120	23833.4	28075.2	84.9 %

data can also determine the crystal size using the Scherrer equation:

$$D = \frac{k\lambda}{B \cos \theta} \quad (7)$$

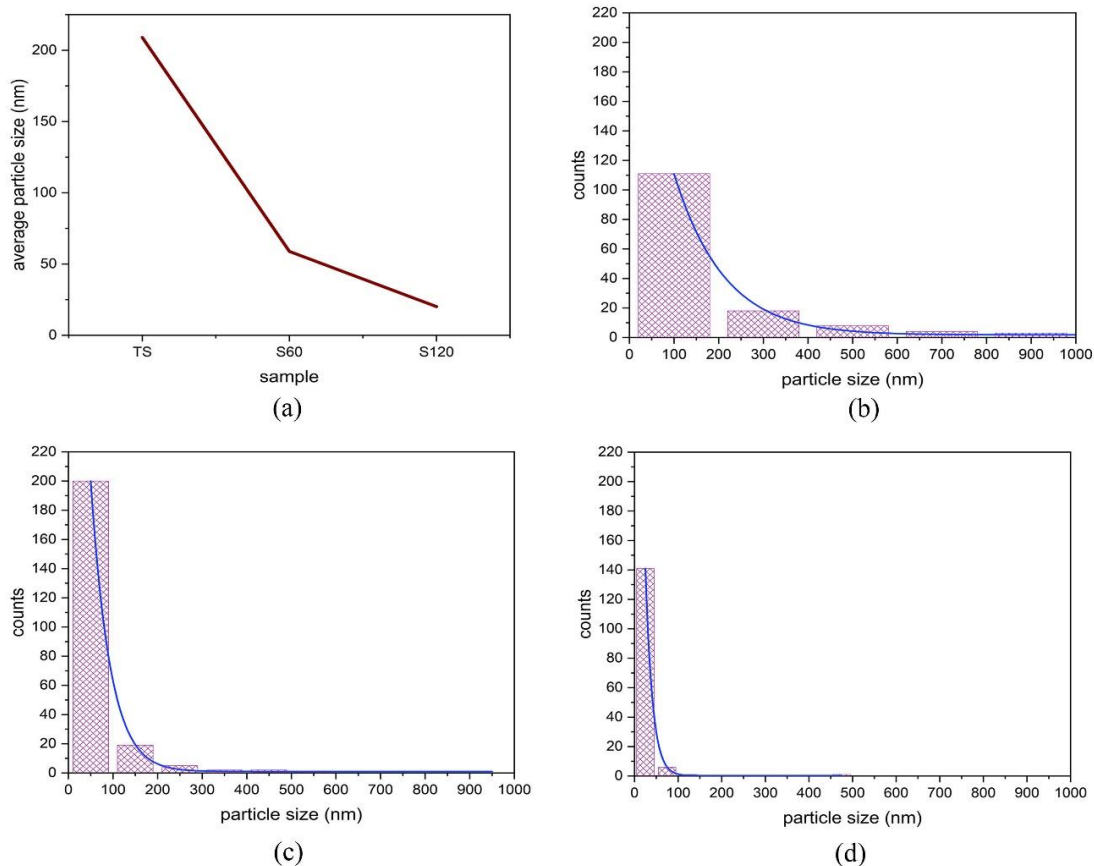
Where D is crystal size (nm), k is Scherrer constant (0,9),  $\lambda$  is Cu wavelength (1,54 nm), and B is curve width.

Table 3 displays the results of the calculation of the silicon crystal size.

**Table 3.** Silicon crystal size

Sample	Crystal Size Range (nm)	Average Crystal Size (nm)
TS	5.9 – 14.2	10.2
S60	6.2 – 13.8	10.4
S120	6.4 – 13.9	10.4

The crystal size calculation data shows that sonication time does not affect crystal size, which means that the energy



**Figure 5.** Average particle size (a), distribution particle of ultrasonication time variation: (b) 0 minutes, (c) 60 minutes, and (d) 120 minutes

Deducting the degree of crystallinity indicates that the structure of the silicon is changing to irregular or amorphous. Anodes of lithium-ion batteries using amorphous silicon nanoparticles show an increase in life cycle compared to crystal nanoparticle silicon [25].

In addition to the degree of crystallinity, XRD intensity

intensity provided by the ultrasonic device frequency of 37 kHz has not been able to shrink the crystal size. The results of the crystal measurement in Table 3 show that the average crystal size is in the range of 10.2-10.4 nm and has no influence on the ultrasonic irradiation power. This shows that the impact of ultrasonic on the nucleation process and the

growth of natural crystals is weak, in line with the research conducted by G. Yang *et al.*, who said that ultrasonic does not influence the size of crystals [18].

Ultrasonication is an effective method for reducing the size and dispersion of nanomaterials during the synthesis process. [18]. Ultrasonication is capable of reducing particle size through cavitation phenomena [26]. When ultrasonic waves pass through the fluid, high and low pressures alternately form and create microscopic bubbles that will break, creating highly energetic conditions that can break the particles into smaller sizes. [27-28].

Figure 5 shows the effects of ultrasonication time on the particle size of silicone samples synthesized from coal ash fly. It shows the sample's particle distribution histogram with ultrasonication time variations. Figure 5 shows the particle size distribution for each silicone sample with non-ultrasonication treatment, 60 minutes of ultrasonication, and 120 minutes of ultrasonication. Figure 5(a) shows the influence of ultrasound time on particle size, where, at the time of the sample without ultrasonication treatment (TS), an average particle size of 208.94 nm was obtained. Ultrasonication with a time of 60 minutes (S60) obtains an average particle size of 58.87 nm, and ultrasonic time of 120 minutes (S120) obtains an average size of particles of 20.13 nm. From these results, it is known that the ultrasonication time affects the particle size.

In Figure 5(b), without ultrasonication treatment, the particle size still has a sufficiently wide range to reach 1000 nm, with most particle sizes distributed in the 500 nm dimensional range. In Figure 5(c), with ultrasonication treatment for 60 minutes, the particle size has a smaller range

**Figure 5.** Average particle size (a), distribution particle of ultrasonication time variation: (b) 0 minutes, (c) 60 minutes, and (d) 120 minutes

below 200 nm. In Figure 5(d), with 120-minute ultrasonication treatment, the particle size is much smaller, mainly below 100 nm, with most particle distribution below 50 nm.

Figure 5 shows that ultrasonication can reduce particle size and make particle size more uniform and homogeneous. This is because the vibration generated by the ultrasonic device can reduce particle size. In general, the mechanism of particle smoothing by ultrasonics can be understood qualitatively based on the style of acoustic radiation and the effects of ultrasonic cavitation [29]. The longer the sonication time, the better the dispersion process, forming more homogeneous nanoparticles [30]. Particle size is an essential basis for designing anodes with high C-rate capabilities, better performance, and lower security risks for lithium-ion batteries [31]. Particle size plays a crucial role in determining the performance of anodes in lithium-ion batteries. Research has shown that varying the particle size of materials like silicon and silicon monoxide significantly impacts their electrochemical behavior. Smaller particles, such as nano-sized silicon, exhibit improved cycle stability and capacity retention due to better stress resistance during charging/discharging, limiting intergranular cracking and

enhancing electron and lithium-ion transport paths [32-34].

## 4. Conclusion

The production of silicon nanoparticles from coal fly ash using ultrasonication presents a promising approach to improve the anode performance of lithium-ion batteries. The extraction of silica from fly ash with a silica content of 49.21% achieved a purity of 93.52%, followed by metallothermic reduction to obtain silicon with a content of up to 61.3%, providing a solid basis for the synthesis of high-quality silicon nanoparticles. Ultrasonication significantly affected the particle size and crystallinity, with longer sonication times producing smaller and more uniform particles. Ultrasonic treatments for 60 and 120 min resulted in average particle sizes of 58.87 nm and 20.13 nm, respectively, compared to 208.94 nm without sonication. This particle size reduction is significant because smaller silicon nanoparticles exhibit better structural stability during lithiation and delithiation processes, which are essential for maintaining high capacity and extending the life cycle of lithium-ion batteries using silicon as the anode material.

## Acknowledgments

The authors want to acknowledge the Renewable Energy Engineering Department, Politeknik Negeri Sriwijaya, and PPM Dit. APTV through Contract No. 55/SPK/D.D4/PPK.01.APTV/III/2024 for funding supports this Master's Thesis Research. The authors also thank

## References

- [1] H. Koshlak, "Synthesis of Zeolites from Coal Fly Ash Using Alkaline Fusion and Its Applications in Removing Heavy Metals," *Materials*, vol. 16, no. 13, Jul. 2023, doi: 10.3390/ma16134837.
- [2] K. M. Zierold and C. Odoh, "A review on fly ash from coal-fired power plants: chemical composition, regulations, and health evidence," *Rev Environ Health*, vol. 35, no. 4, pp. 401–418, Nov. 2020, doi: 10.1515/reveh-2019-0039.
- [3] T. M. A. Mokgehie, W. M. Gitari, and N. T. Tavengwa, "Synthesis and Characterization of Zeolites Produced by Ultrasonication of Coal Fly Ash/NaOH Slurry Filtrates," *South African Journal of Chemistry*, vol. 73, 2020, doi: 10.17159/0379-4350/2020/v73a10.
- [4] K. Karmaili *et al.*, "Chemical Composition Study of Coal Ash Content as Potential," *Konversi*, vol. 12, no. 2, Oct. 2023, doi: 10.20527/k.v12i2.16592.
- [5] S. Kamara, E. H. Foday Jr, and W. Wang, "A Review on the Utilization and Environmental Concerns of Coal Fly Ash," *American Journal of Chemistry and Pharmacy*, vol. 2, no. 2, pp. 53–65, Jul. 2023, doi: 10.54536/ajcp.v2i2.1609.

- [6] V. K. Yadav and P. R. Pandita, "Fly Ash Properties and Their Applications as a Soil Ameliorant," 2019, pp. 59–89. doi: 10.4018/978-1-5225-7940-3.ch005.
- [7] B. K. Shukla, A. Gupta, S. Gowda, and Y. Srivastav, "Constructing a greener future: A comprehensive review on the sustainable use of fly ash in the construction industry and beyond," *Mater Today Proc*, vol. 93, pp. 257–264, 2023, doi: 10.1016/j.matpr.2023.07.179.
- [8] Y. Bow, A. Hasan, R. Rusdianasari, Z. Zakaria, B. Irawan, and N. Sandika, "Biodiesel from Pyrolysis Fatty Acid Methyl Ester (FAME) using Fly Ash as a Catalyst," *Proceedings of the 5<sup>th</sup> FIRST T1 T2 2021 International Conference (FIRST-T1-T2 2021)*, 9, 175-181. <https://doi.org/10.2991/ahe.k.220205.030>.
- [9] A. Xing, J. Zhang, R. Wang, J. Wang, and X. Liu, "Fly ashes as a sustainable source for nanostructured Si anodes in lithium-ion batteries," *SN Appl Sci*, vol. 1, no. 2, p. 181, Feb. 2019, doi: 10.1007/s42452-019-0196-y.
- [10] T. Kim and J. Lee, "Silicon nanoparticles: fabrication, characterization, application and perspectives," *Micro and Nano Systems Letters*, vol. 11, no. 1, p. 18, Nov. 2023, doi: 10.1186/s40486-023-00184-9.
- [11] T. Sujati, T. Dewi, and R. Rusdianasari, "Charging System Design of a Solar Powered Mobile Manipulator," in *Proceedings - IEIT 2021: 1st International Conference on Electrical and Information Technology*, Institute of Electrical and Electronics Engineers Inc., Sep. 2021, pp. 179–184. doi: 10.1109/IEIT53149.2021.9587401.
- [12] J. Lee, G. Oh, H.-Y. Jung, and J.-Y. Hwang, "Silicon Anode: A Perspective on Fast Charging Lithium-Ion Battery," *Inorganics (Basel)*, vol. 11, no. 5, p. 182, Apr. 2023, doi: 10.3390/inorganics11050182.
- [13] M. K. Majeed et al., "Silicon-based anode materials for lithium batteries: recent progress, new trends, and future perspectives," *Critical Reviews in Solid State and Materials Sciences*, vol. 49, no. 2, pp. 221–253, Mar. 2024, doi: 10.1080/10408436.2023.2169658.
- [14] A. Taqwa and Y. Bow, "Monitoring Depth of Discharge of a Valve Regulated Lead Acid Battery in a Standalone PV System," 2021. 4<sup>th</sup> Forum in Research, Science, and Technology, 233-237.
- [15] N. Joudeh and D. Linke, "Nanoparticle classification, physicochemical properties, characterization, and applications: a comprehensive review for biologists," *J Nanobiotechnology*, vol. 20, no. 1, p. 262, Jun. 2022, doi: 10.1186/s12951-022-01477-8.
- [16] Y. Khan et al., "Classification, Synthetic, and Characterization Approaches to Nanoparticles, and Their Applications in Various Fields of Nanotechnology: A Review," *Catalysts*, vol. 12, no. 11, p. 1386, Nov. 2022, doi: 10.3390/catal12111386.
- [17] H. Lu et al., "Modular and Integrated Systems for Nanoparticle and Microparticle Synthesis—A Review," *Biosensors (Basel)*, vol. 10, no. 11, p. 165, Nov. 2020, doi: 10.3390/bios10110165.
- [18] G. Yang et al., "Understanding the relationship between particle size and ultrasonic treatment during the synthesis of metal nanoparticles," *Ultrason Sonochem*, vol. 73, p. 105497, May 2021, doi: 10.1016/j.ultsonch.2021.105497.
- [19] D. Dhaneswara, J. F. Fatriansyah, F. W. Situmorang, and A. N. Haqoh, "Synthesis of Amorphous Silica from Rice Husk Ash: Comparing HCl and CH<sub>3</sub>COOH Acidification Methods and Various Alkaline Concentrations," *International Journal of Technology*, vol. 11, no. 1, pp. 200–208, Jan. 2020, doi: 10.14716/ijtech.v11i1.3335.
- [20] Q.-W. Zhang, L.-G. Lin, and W.-C. Ye, "Techniques for extraction and isolation of natural products: a comprehensive review," *Chin Med*, vol. 13, no. 1, p. 20, Dec. 2018, doi: 10.1186/s13020-018-0177-x.
- [21] Y. Tan, T. Jiang, and G. Z. Chen, "Mechanisms and Product Options of Magnesiothermic Reduction of Silica to Silicon for Lithium-Ion Battery Applications," *Front Energy Res*, vol. 9, Mar. 2021, doi: 10.3389/fenrg.2021.651386.
- [22] D. Kumar and M. Johari, "Characteristics of silicon crystal, its covalent bonding and their structure, electrical properties, uses," 2020, p. 040037. doi: 10.1063/5.0003505.
- [23] X. Yang and Q. Zhan, "Investigation on the electrical and optical properties of forsterite Mg<sub>2</sub>SiO<sub>4</sub> under pressure up to 30 GPa," *Mol Simul*, vol. 46, no. 11, pp. 805–811, Jul. 2020, doi: 10.1080/08927022.2020.1714611.
- [24] A. Raza, S. Y. Kim, J. Choi, J. Kim, M. Park, and S. Lee, "Crystallinity-controlled SiO<sub>x</sub> anode material prepared through a salt-assisted magnesiothermic reduction for lithium-ion batteries," *Int J Energy Res*, vol. 46, no. 13, pp. 18269–18277, Oct. 2022, doi: 10.1002/er.8443.
- [25] A. Ulvestad et al., "Crystallinity of Silicon Nanoparticles: Direct Influence on the Electrochemical Performance of Lithium Ion Battery Anodes," *ChemElectroChem*, vol. 7, no. 21, pp. 4349–4353, Nov. 2020, doi: 10.1002/celec.202001108.
- [26] A. Pratap-Singh, Y. Guo, S. Lara Ochoa, F. Fathordoobady, and A. Singh, "Optimal ultrasonication process time remains constant for a specific nanoemulsion size reduction system," *Sci Rep*, vol. 11, no. 1, p. 9241, Apr. 2021, doi: 10.1038/s41598-021-87642-9.
- [27] J. A. Morton et al., "Dual frequency ultrasonic cavitation in various liquids: High-speed imaging and acoustic pressure measurements," *Physics of Fluids*, vol. 35, no. 1, Jan. 2023, doi: 10.1063/5.0136469.
- [28] K. Bauckhage, "Atomization of Liquids with Widely Differing Material Properties by Ultrasonic Standing-Waves," in *Proceedings of the Seventh International Conference on Liquid Atomization and Spray Systems*, Connecticut: Begellhouse, 2023, pp. 601–608. doi: 10.1615/ICLASS-97.740.
- [29] S. S. Sabnis, R. Raikar, and P. R. Gogate, "Evaluation of different cavitation reactors for size reduction of DADPS," *Ultrason Sonochem*, vol. 69, p. 105276, Dec. 2020, doi: 10.1016/j.ultsonch.2020.105276.
- [30] N. Rofiqoh et al., "Effect of Sonication Time and Particle Size for Synthesis of Magnetic Nanoparticle from Local Iron Sand," 2020. [Online]. Available: <https://www.researchgate.net/publication/341735837>
- [31] L. Bläubaum, F. Röder, C. Nowak, H. S. Chan, A. Kwade, and U. Krewer, "Impact of Particle Size Distribution on Performance of Lithium-Ion Batteries," *ChemElectroChem*, vol. 7, no. 23, pp. 4755–4766, Dec. 2020, doi: 10.1002/celec.202001249.
- [32] J. Müller, P. Michalowski, and A. Kwade, "Impact of Silicon

Content and Particle Size in Lithium-Ion Battery Anodes on Particulate Properties and Electrochemical Performance,” *Batteries*, vol. 9, no. 7, p. 377, Jul. 2023, doi: 10.3390/batteries9070377.

- [33] F. Wu et al., “Benchmarking the Effect of Particle Size on Silicon Anode Materials for Lithium-Ion Batteries,” *Small*, vol. 19, no. 42, Oct. 2023, doi: 10.1002/sml.202301301.
- [34] S. Yi et al., “Insights into the Effect of SiO Particle Size on the Electrochemical Performance between Half and Full Cells for Li-Ion Batteries,” *ACS Appl Mater Interfaces*, vol. 15, no. 20, pp. 24377–24386, May 2023, doi: 10.1021/acsami.3c01418.